Oil-water receiving membrane with sub-10 nm surfactant layer for long-lasting oil-water separation

Yajie Ding[a†], Nianxiang Qiu[d†], Jianqiang Wang[a,b]*, Zhe Yang[c], Fu Liu[a,b]*, Chuyang Y. Tang[c]

[a]Key Laboratory of Marine Materials and Related Technologies, Zhejiang Key Laboratory of Marine Materials and Protective Technologies, Ningbo Institute of Materials Technology and Engineering, Chinese Academy of Sciences, Ningbo, P. R. China;

[b]University of Chinese Academy of Sciences, Beijing, P. R. China;

[c]The University of Hong Kong, Hong Kong, P. R. China.

[d]Engineering Laboratory of Nuclear Energy Materials, Ningbo Institute of Materials Technology and Engineering, Chinese Academy of Sciences, Ningbo, Zhejiang, 315201, PR China.

E-mail: wangjianqiang@nimte.ac.cn; fu.liu@nimte.ac.cn

Graphical Abstract

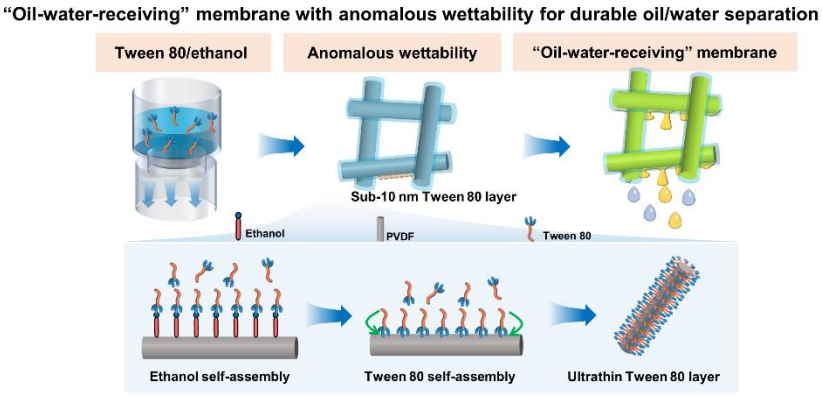

Abstract: Oil fouling is an inherent threaten of membrane-based separation of oil-water emulsion, while common physical sieving membrane separation and coalescence demulsification fail to achieve long term applications and combat severe water flux declines. We hereby report an "oil-water-receiving" membrane with anomalous wettability constructed by sub-10 nm Tween 80 assembly on hydrophobic PVDF nanofibers to establish independent water and oil transmembrane passageway. Water can go through the membrane freely along the hydrophilic nanofiber surface. While emulsified oils were diverted beneath the ultra-thin hydrophilic layer and captured by PVDF bulk to form coalesced oil phase and discharged out of the nanofibrous membrane as continuous macroscopic oil phase. The membrane showed stable permeate flux as high as 536 ± 40 L m^{-2} h^{-1} bar^{-1} after 10 h of continuously filtering oil-in-water emulsions. The conformation assembly of surfactants with hydrophilic and hydrophobic chains provides a new strategy to fabricate anti-fouling membranes for oil/water separation.

Key words

Oil fouling, "oil-water-receiving" membrane, anomalous wettability, independent water and oil transmembrane passageway

1. Introduction

Membranes with superwetting interfaces have been widely exploited in recent years[1]. Commonly, superhydrophilic or superhydrophobic interface exhibited underwater superoleophobic property or under oil superhydrophobic property. Based on this unique characteristic, superwetting membranes have been widely used for oil/water separation[2]. Quite high membrane flux and separation efficiency can be obtained by manipulating physicochemical properties of membranes. However, membrane fouling is a huge challenge in the oil/water separation process, which causes a rapid reduction in membrane permeability within minutes[3, 4]. Therefore, continuous emulsion separation process calls for a novel antifouling strategy due to the inevitable constraints.

Membrane fouling in oil/water separation process was mainly caused by the physical sieving mechanism, where the dispersed phase tends to absorb on membrane surface[5, 6]. For removing the fouling layer, several coupling strategies have been reported[7, 8], such as physical/chemical cleaning[9, 10], catalytic degradation[11-17], *in-situ* microbubbles[18-20] and pyrolysis[21, 22] etc. Notwithstanding high permeance recovery, requirements of additional chemicals, off-line operations, and thermal resistance of membrane materials greatly limited the application. Membrane coalescence demulsification offers an alternative method of decontamination[23-26]. In this process, emulsified oil is adsorbed/collided on the hydrophobic/hydrophilic pore surface, coalesced and subsequently flowed away from membrane by continuous water phase.

Unfortunately, the coalesced oils cannot be completely removed because the coalesced oil droplets are easily deformed and have strong affinity towards hydrophobic channel surfaces. We proposed that membranes with tunable hydrophilic

component (e.g., polyhydroxyethyl methylacrylate, PHEMA) could restrain oil fouling during coalescence demulsification process[27]. Separation permeance of membrane was stable during 2 h of continuous separation without cleaning. Incorporated PHEMA played an important role of enhancing antifouling property of membrane due to hydration layer formed by PHEMA, similar to the case of superhydrophilic membranes[28-32]. The hydrated channel wall repelled demulsified oils and forced them to aggregate in membrane channels (hydrophilic and oil-repellent)[33]. However, membrane channels occupied 60%-95% of the membrane volume and once membrane channels were blocked by the oils, fouling occurred. Therefore, the avoiding of oil aggregation in membrane channels is the gold key for solving membrane fouling. To achieve this target, the anomalous wettability of membrane pore surface needs be designed different from common hydrophilic or/and underwater oleophobic property.

In this study, membrane with anomalous superhydrophilic and underwater superoleophilic property was constructed by sub-10 nm hydrophilic layer on PVDF nanofibers through simple surfactant molecular assembly. Benefit from this unique wetting property, water and demulsified oils can freely go through membrane ("oil-water-receiving") without oil retention. Meanwhile, demulsified oils can be diverted to the beneath PVDF nanofiber surface through the ultrathin surfactant layer for further coalescence and release. Therefore, the pore plugging by oils are facilely liberated for enhanced membrane antifouling performance. The ultrathin hydrophilic layer strategy offered new understanding for oil/water separation through coalescence demulsification and will significantly advance its practical applications.

2. Experimental

2.1 Chemicals and materials

Poly(vinylidene fluoride) (PVDF, average Mw: 180000, pellets), polystyrene (PS, average Mw: 192000), polycaprolactone (PCL, Mw: 80000) were ordered from

Sigma-Aldrich (America). Decamethylcyclopentasiloxane (D5), dodecane, hexadecane, Span 80, Span 20, Span 85, Tween 20, Rhodamine B, sodium laurylsulfonate (SLS, 98%), dopamine hydrochloride was purchased from Aladdin Biochemical Technology Co., Ltd. (China). Polyurethane (PU, 1180A) was brought from BASF Corporation (Germany). Tween 80, N, N-dimethylformamide (DMF), anhydrous ethanol, trifluoroethanol (TFEA), chloroform, n-butanol, toluene, hydrochloric acid, sodium hydroxide was obtained from Sinopharm Chemical Reagent Co., Ltd (China), Tween 85 was purchased from Shanghai Macklin Biochemical Co., Ltd (China). Decamethylcyclopentasiloxane (D5, ≥97%) was purchased from Trellis Trade Inc. (China). All chemicals were used as received without further purification.

Nanofibrous membrane preparation. Different nanofibrous membranes were fabricated via electrospinning method. PVDF nanofibrous membrane was prepared based on our previously reported method[34]. Typically, 25 wt% homogeneous PVDF/DMF solution was used for electrospinning. The injection speed, applied voltage and receiving distance are 1.0 mL h^{-1}, 16 kV and 15 cm, respectively. Speed of the receiver is 80 rpm. The thickness of nanofibrous membrane in this work is 120±5 μm. Preparation parameters of other nanofibrous membrane (PS, PSF, PCL, PU) were shown in Table S2.

2.2 Preparation of the TPVDF nanofibrous membrane

Electrospun PVDF nanofibrous membrane was sandwiched between two filter cups, and then a certain concentration of Tween 80/ethanol solution (0.1, 0.5, 1.0, 1.5, 2.0, 3.0, 5.0, 7.0, 10.0 g L^{-1}) was filtered through the membrane under gravity condition for a certain time (5, 10, 30, 60, 90, 120, 150 min). Without special instructions, Tween 80 concentration and filtration time is 5 g L^{-1} and 2 h respectively. The obtained membrane was named as TPVDF. For comparison, ethanol treated PVDF nanofibrous membrane in the same way for 2 h was named as EPVDF. A schematic diagram of the preparation process of TPVDF membrane was presented in Figure 1a.

2.3 Preparation of the HTPVDF nanofibrous membrane

5 g L^{-1} Tween 80/hexane solution was filtered through the membrane under gravity condition for 2 h. The obtained membrane was named as HTPVDF.

2.4 Characterizations

Surface morphologies of membranes were photographed by cold-field emission scanning electron microscopy (SEM, S4800, Hitachi, Japan). Transmission electron microscopy (TEM, Talos F200X, Thermo Fisher, USA) with EDAX was used to observe structure and element distribution of nanofibers. To prepare TEM samples, firstly, we stick the aluminum foil paper onto the receiving device and keep the end at a certain distance from the receiving device. Secondly, electrospun for 30 s according to the corresponding parameters. Thirdly, use a copper mesh to pick up the nanofibers between the aluminum foil paper and the receiving device. Finally, the copper mesh containing nanofibers was modified using the same method. Contact angle meter (OCA25, Dataphysics, Germany) was employed to analyze wetting property. Vis spectrophotometer (Lambda 950, PerkinElmer, USA) and microscopic infrared spectrometer (Micro-FTIR, Cary660+620, Agilent, USA) was used to analyze functional group of the membranes. Thermogravimetry analyzer/differential thermal comprehensive thermal (Diamond TG/DTA, PerkinElmer, USA) was used to analyze the content of surfactant on nanofibrous membrane. X-ray powder diffractometer (XRD, D8 ADVANCE, BRUKER AXS, Germany) was used to measure the crystal form of PVDF. Quartz crystal microbalance (QCM-D, Biolin Scientific, Sweden) was used to measure adsorption and desorption of surfactants on membrane. Polarized hot stage microscope (BX51, OLYMPUS, Japan) and dynamic light scattering particle size analyzer (Zetasizer Nano ZS, Malvern, Britain) was applied to measure size distribution of emulsion. TOC Analyzer (Multi N/C 3100, Analytik Jena AG, Germany) was employed to detect the content of oil in feed and filtrate.

2.5 Determination of thickness and content of surfactant on nanofibers

PVDF nanofibers coated sensors were obtained by electrospinning 25 wt% PVDF/DMF solution onto a gold sensor at the rate of 1.0 mL h^{-1} for 4 h. The sensor was then put into an open test cell (Biolin Scientific). Before tests, ethanol or hexane

was passed over the sensor until a stable baseline was acquired. After that, kinetic experiments were conducted by flowing 5 g L^{-1} Tween 80/ethanol or Tween 80/hexane solution through the QCM-D for 2 h. Desorption experiments were conducted by changing the test solution to deionized water for 8 h. The mass and thickness of the loaded Tween 80 was characterized by the frequency change through the Sauerbrey equation.

$$\Delta m = \frac{-C\Delta f}{n}$$

$$\Delta \delta = \frac{\Delta m}{100}$$

where Δf is the frequency change (Hz), C is a constant (17.7 ng cm^{-2} Hz^{-1}), n is the resonance overtone number, Δm (ng cm^{-2}) and $\Delta \delta$ (nm) is the mass and thickness of loaded surfactant, respectively.

2.6 Oil-in-water emulsion separation

SLS-stabilized oil-in-water emulsion was firstly prepared before separation. Concentration of SLS and oil was 0.1 g L^{-1} and 1.0 vol% respectively. The mixed solution was mechanically stirred for 6 h to form a milky white stable emulsion (stable at least 24 h). A home-made cross-flow filter apparatus with a cell of 2.8 cm in diameter was used to estimate the separation performance of membranes. The membrane needs to be pre-impregnated with water before separation and the operating pressure was set at 0.2 bar. Volume of filtrate was recorded every 20 min to evaluate permeation flux.

2.7 Molecular dynamics simulation

All molecular dynamics (MD) simulations were performed using large scale atomic/molecular massively parallel simulator, distributed as an open code for massively parallel simulations[35]. Molecular visualization was performed using Visual Molecular Dynamics (VMD) tool[36] and Materials Studio software. The simulation configurations for molecular dynamics simulations were created by packing optimization via the Packmol code[37]. Short-range interactions were calculated with a cutoff distance of 12 Å, whereas the coulombic long-range

interactions were calculated using the PPPM algorithm[38]. Nose-Hoover thermostat[39] was used to control the temperature of 300 K, and Berendsen barostat[40] was applied to control the pressure of 1 atm for MD simulations. The simulation time step was set to 1 fs. Periodic boundary conditions were imposed in all three Cartesian directions.

Polyvinylidene fluoride (PVDF) chain ($C_{100}H_{102}F_{100}$, shown in Figure S26, Supporting Information) was modeled as a 50-mer unit. The bonded and non-bonded parameters of PVDF were taken from an explicit-hydrogen all-atom model based on the OPLS-AA force-field of $C_{16}H_{18}F_{16}$ molecule[41, 42]. However, in order to maintain the zero charge of each subunit and allow the connection between these subunits, the partial charge of each atom of PVDF was adjusted as shown in Figure S25, Supporting Information. The molecular structures of (a) PVDF chain, (b) Tween 80, (c) ethanol and (d) hexane. White, red, cyan and gray colors represent the H, O, F and C atoms, respectively. An amorphous cell comprised of 60 PVDF chains was constructed and minimized, followed by a 5 ns NPT run to reach the real density and obtain equilibrium PVDF structure.

Tween 80, hexane and ethanol molecules were all represented by the OPLS-AA force-field, while the partial charge per atom of Tween 80 were determined by an automated force field Topology Builder (ATB) method[43]. Three PVDF-Tween 80-solvent initial MD systems were constructed, all containing the PVDF structure and 20 Tween 80 molecules placed on PVDF surface in a simulation box with dimensions of 80 Å × 80 Å × 180 Å, the first one with an additional 5000 ethanol molecules to solvate the Tween 80 molecules (Figure S27a, Supporting Information), the second one with an additional 5000 hexane molecules (Figure S27b, Supporting Information), and the third one without any solvent molecules (Figure S27c, Supporting Information). After that, the three MD models were minimized and then performed through a 50 ns NVT simulation to mimic the adsorption of Tween 80 molecules onto the PVDF polymers.

3. Results and discussion

3.1. Superhydrophilic and underwater superoleophilic interface construction.

Interfaces with superhydrophilic and underwater superoleophobic properties are easily realized and have been widely reported[44-48]. However, interfaces with superhydrophilic and underwater superoleophilic properties are anomalous. However, we are able to achieve this unique surface property simply by elaborately tuning the thickness of hydrophilic layer on PVDF nanofibers. Surfactant (e.g., Tween 80)/ethanol solution was filtrated through a hydrophobic PVDF nanofibrous membrane under gravity (Figure 1a). Ethanol was chosen as the solvent due to its fast-wetting property to PVDF (Figure S1a, Supporting Information) and high solubility for Tween 80 (Figure S1b, Supporting Information). The interfacial tension of Tween 80/ethanol solution was stable in a wide concentration range (5-300 g L^{-1}, Figure 1b)[49]. During filtration, ethanol molecules adsorbed on PVDF nanofiber through hydrophilic hydroxyl groups exposed to the solution. Herein, ethanol exhibited feature of surfactant to some extent due to its ethyl and hydroxyl group in chemical structure[50]. Hydrophilic segments of Tween 80 molecules then contacted with the exposed hydroxyl groups of ethanol due to their strong interaction[51]. After filtration, a little amount of Tween 80/ethanol solution was left on the surface of PVDF nanofiber. Ultrathin Tween 80 molecules were finally assembled on PVDF nanofiber surface due to the evaporation of ethanol. Binding force between Tween 80 and PVDF might be the hydrophobic interaction (detailed information can be found in molecular dynamic simulation section). A schematic diagram about the Tween 80 coating on PVDF nanofiber was shown in Figure 1c.

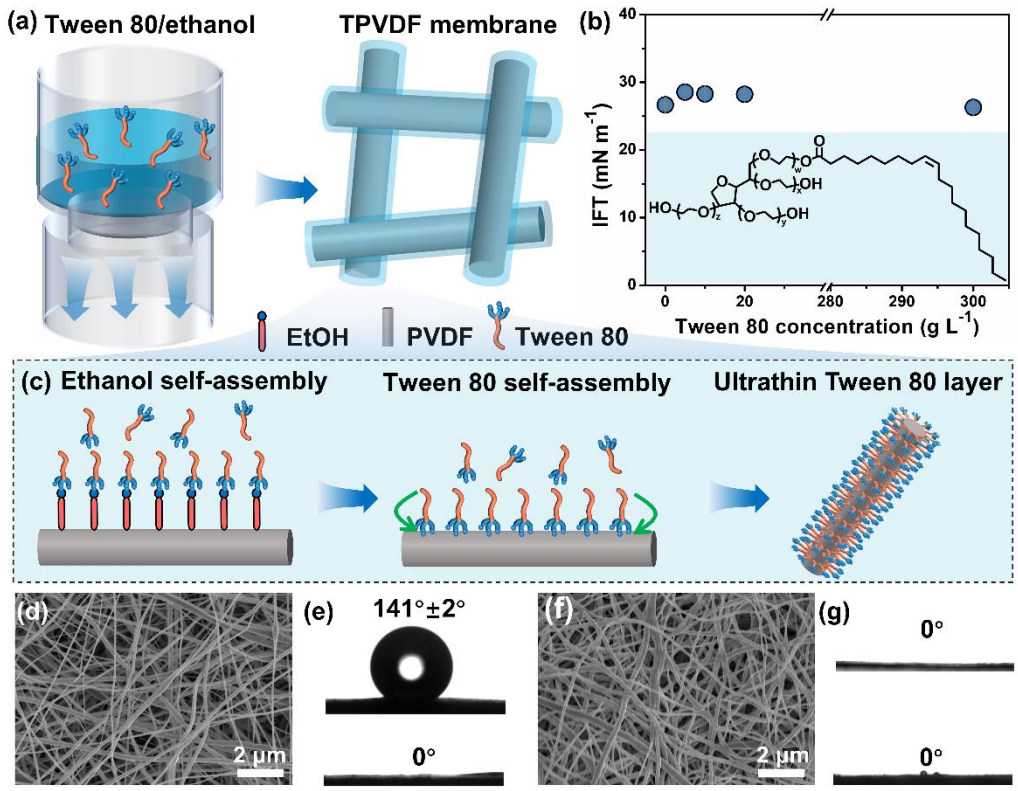

Figure 1. Tween 80 assembly on hydrophobic PVDF nanofibrous membrane to form oil-water-receiving membrane with superhydrophilic in air and superlipophilic underwater. Schematic illustrations of (a**)** preparation of TPVDF nanofibrous membrane, (b) Surface tension of ethanol as a function of Tween 80 concentration. (c) Tween 80 was self-assembled on the surface of hydrophobic PVDF nanofiber to form an ultrathin surfactant layer. SEM micrographs of (d) pristine PVDF and (f) TPVDF nanofibrous membrane. Water/oil contact angles of (e) PVDF and (g) TPVDF nanofibrous membrane in air/underwater.

PVDF nanofibrous membrane was composed of randomly stacked nanofibers (Figure 1d). Water contact angle and underwater oil contact angle of PVDF nanofibrous membrane was about $141^o \pm 2^o$ and 0^o respectively (Figure 1e). After filtration of Tween 80/ethanol solution, TPVDF exhibited a more tightly packed structure (Figure 1f). The water (upper) and underwater oil (below) contact angle was all 0^o (Figure 1g, SV1), which was anomalous to common sense[52-56]. The formation may be due to the presence of an ultrathin hydrophilic Tween 80 layer on the surface of hydrophobic

PVDF nanofiber: 1) A self-assembly of Tween 80 with the hydrophilic segments exposing to the external environment at the interface of PVDF nanofibers (super-hydrophilic in air); 2) Ultrathin hydrophilic Tween 80 layer and hydrophobic PVDF nanofiber matrix form Janus-like structure, which allows underwater oil droplets enter the hydrophobic PVDF nanofiber from the ultrathin hydrophilic Tween 80 layer through the Laplace force (directional penetration, underwater superlipophilic). This unique wetting property can be obtained in a wide range of Tween 80 concentration (1.5-10.0 g L^{-1}, Figure S2a, Supporting Information). Water wetting time was significantly decreased from 140 ms to 5 ms with increasing the concentration (Figure S2b, Supporting Information). Moreover, if relatively high Tween 80 concentration was used (e.g., 5 g L^{-1}), the filtration time can be decreased to 5 min for obtaining superhydrophilic and underwater superoleophilic property (Figure S2c, Supporting Information). In addition, no obvious surface morphology change was found at different Tween 80 concentrations (Figure S3, Supporting Information). Notably, superhydrophilic and underwater superoleophilic property cannot be achieved if Tween 80 concentration was lower than 1.5 g L^{-1} (e.g., 0.1-1.0 g L^{-1}, Figure S2a, Supporting Information).

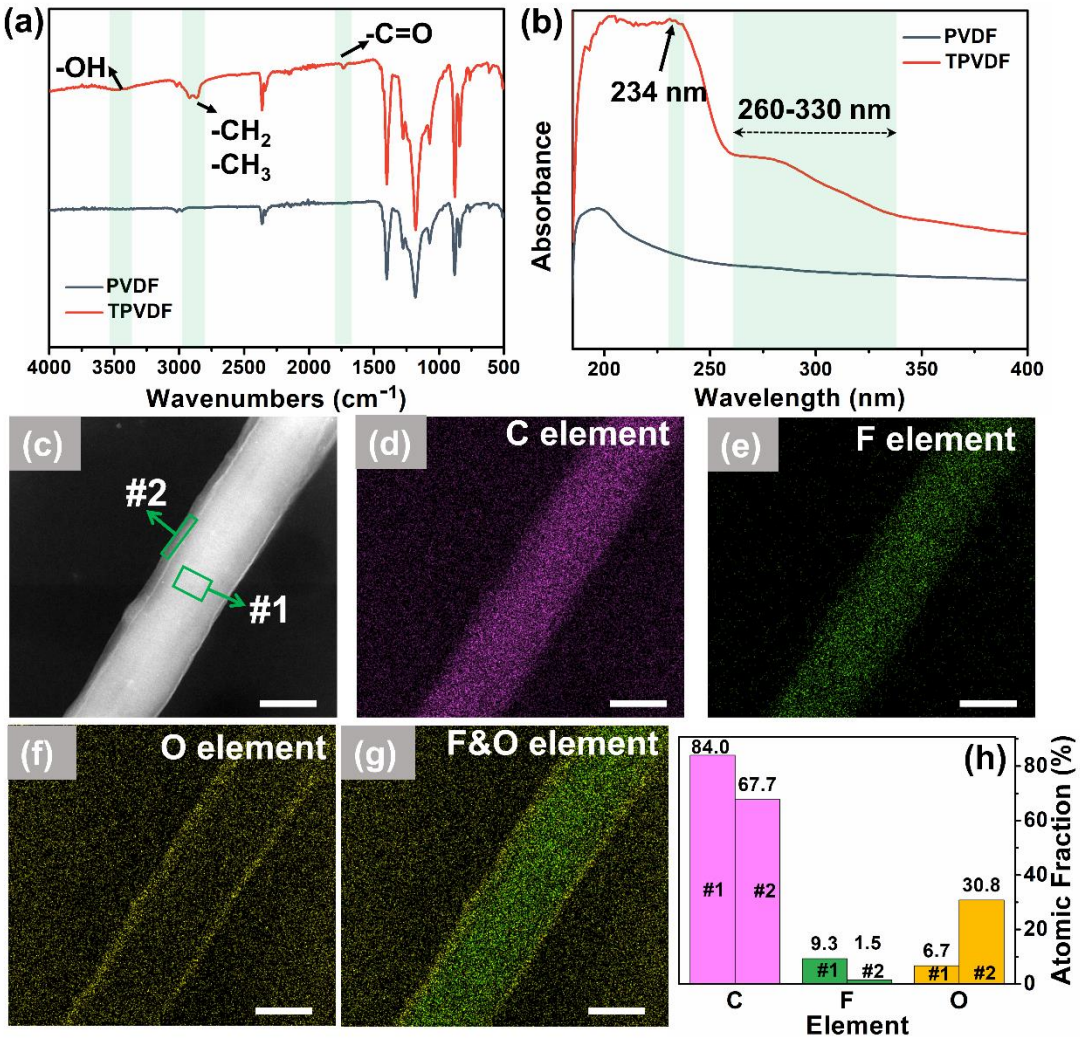

Figure 2. Chemical composition of TPVDF nanofibrous membrane. ATR-FTIR (a) and (b) UV-Vis spectra of the PVDF and TPVDF nanofibrous membranes. (c-g) EDX scanning images of TPVDF nanofibrous membrane: (d) C element, (e) F element, (f) O element, and (g) F, O double element on the surface. (h) The content of elements at different positions in Figure 2c. The scale bar in Figure 2c-2g is 100 nm.

New stretching vibration peak of -OH and -C=O group at 3440 and 1735 cm^{-1} in ATR-FTIR spectrum suggested the appearance of Tween 80 molecules on PVDF nanofiber (Figure 2a)[57, 58]. In addition, new absorption peaks at 234 nm and the peaks in the region of 260 nm to 330 nm also suggested the presence of Tween 80 (Figure 2b). To get a more visible and direct observation of Tween 80 layer on PVDF

nanofiber, TEM-EDX elemental mapping was carried out. Results in Figure 2c-2g indicated that a uniform Tween 80 layer was anchored on the surface of PVDF nanofiber. Compared to PVDF nanofibrous membrane (O: 4.0 wt%, F: 14.5 wt%, Figure S4, Supporting Information), the content of O element in TPVDF nanofibrous membrane was increased to 6.7 wt% and 30.8 wt% in #1 and #2 area respectively. Meanwhile, the content of F element was decreased to 9.3 wt% and 1.5 wt% correspondingly (Figure 2h). Moreover, a clear enrichment of O element in the outer surface can be observed in Figure 2f, while F and C element was mainly distributed on the main nanofiber (Figure 2d, e and g). Benefit from the interaction between Tween 80 and RB[59], RB was used to validate the Tween 80 loading on membrane surface. CLSM results in Figure S5, Supporting Information showed that bright green fluorescence covered the whole surface of the TPVDF, while weak fluorescence exists in PVDF. The reason was mainly attributed to the hydrophobic property of PVDF membrane. All the results confirmed the presence of Tween 80 layer on PVDF nanofiber.

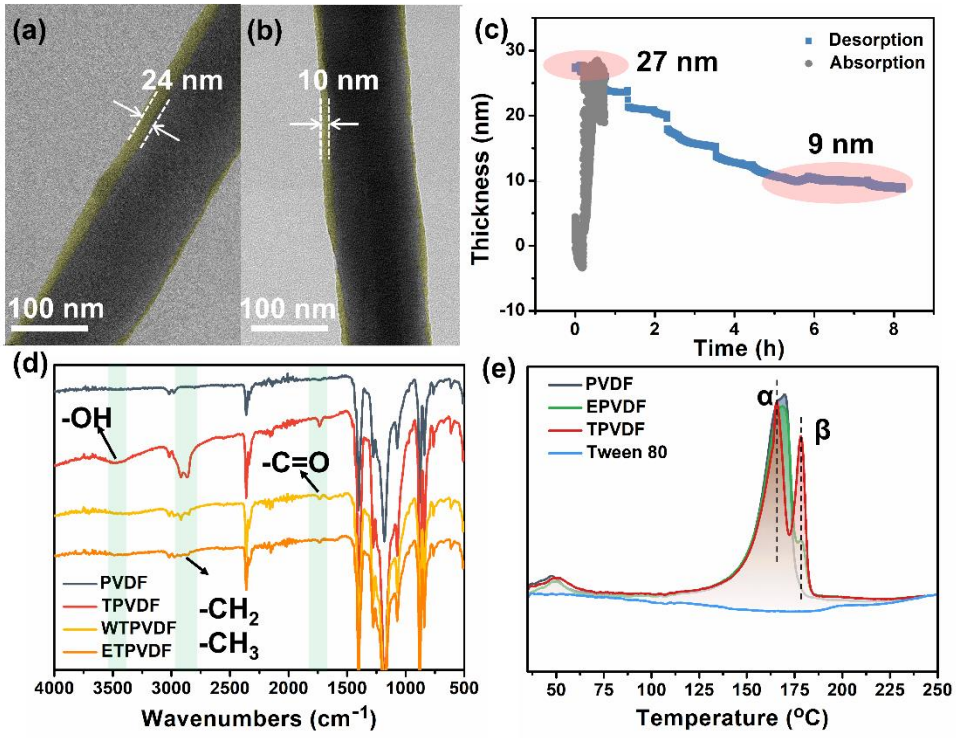

Figure 3. Thickness and stability of Tween80 on PVDF nanofibers. TEM images of TPVDF nanofibrous membrane before (a) and after (b) cleaning. (c) Adsorption and desorption of Tween 80 onto PVDF nanofibrous membrane in ethanol measured by QCM-D. (d) ATR-FTIR spectrums of the TPVDF membrane after being washed in water/ethanol (WTPVDF/ETPVDF) at 120 rpm for 7 days. (e) DSC spectra of PVDF, EPVDF, TPVDF and Tween 80. The yellow stained area is the Tween 80 layer.

Thickness of Tween 80 layer on PVDF nanofiber was directly observed by TEM, which was about 24 nm (Figure 3a). The experimental results fit the Freundlich isotherm model (R^2=0.99198) as compared to the Langmuir model (R^2=0.9888) (Figure S6a, Supporting Information). After thorough cleaning with ethanol for 24 h, the isotherm adsorption curve conforms to Langmuir model (R^2=0.96898) and the final thickness of Tween 80 layer was about 10 nm (Figure S6b, Supporting Information, Figure 3b). To further quantitatively explore the thickness and mass of Tween 80 on PVDF nanofibrous membrane, QCM-D testing was carried out. Results in Figure 3c indicated that an initial thickness of 27 nm over the course of 2 h of adsorption. Then, it was leveled off at about 9 nm after 8 h desorption. This phenomenon suggests that there was a maximum and stabilized value for the Tween 80 thickness, which was basically consistent with the results of TEM results. The quantitative results of Tween 80 on PVDF nanofibrous membrane were decreased from 2700 to 900 ng cm^{-2} correspondingly (Figure S7, Supporting Information). TEM and QCM-D results confirmed that the assembled Tween 80 layer on PVDF nanofiber was quite thin (~ 10 nm). The long-term stability of Tween 80 layer was evaluated through thorough water and ethanol washing at 120 rpm for 7 days. ATR-FTIR results in Figure 4d indicated that characteristic absorption peaks (3440 and 1735 cm^{-1}) of Tween 80 can be clearly identified after water or ethanol washing. Water contact angle and underwater oil contact angle of membrane after washing was unchanged (Figure S8, Supporting Information). It is revealed that the superhydrophilic and underwater superoleophilic feature could stably maintain even after 10 h of cross-flow filtration

(Figure S9, Supporting Information).

To understand the mechanism of stable anchoring of Tween 80 on PVDF membrane, we examined the changes in PVDF crystalline shape after ethanol and Tween 80 treatment by XRD and DSC. PVDF membrane (Figure S10, Supporting Information) are mainly in the α phase and β phase, as shown by the intense peaks at 14.6° and 20.7°, corresponding to the crystal of nonpolar α-phase and the orthorhombic β-phase reflections in 100 and 110/200 planes[60, 61]. The relative quantities of the β-phase and α-phase in the PVDF nanofibrous membrane were determined as a function of ethanol and Tween 80. The β-phase/α-phase ratio of PVDF nanofibrous membrane was enhanced after ethanol and ethanol-Tween 80 treatment (Figure S11, Supporting Information)[62]. These results indicated that the ethanol and Tween 80 played a significant role in enhancing the β-phase content of the crystals. Ethanol was negatively charged due to the presence of hydroxo-groups. The positive CH_2 dipoles (δ^+) in the PVDF chains forms an ion-dipole interaction with the negatively charged ethanol, facilitating the formation of β-phase crystals[63, 64]. Tween 80 is an amphiphilic molecule and its hydrophobic group has hydrophobic interaction with PVDF[65]. Further, Tween 80 reduced the surface energy of PVDF and promoted the interaction between ethanol-Tween 80 and PVDF[66]. Therefore, Tween 80 could be stably attached to β-PVDF due to the polar interaction. Figure 3e illustrates DSC heating curves of pure PVDF, EPVDF, and TPVDF nanofibrous membrane. For PVDF, the melting point was 169.9 ℃ and the crystallinity was 25.2%. A wide peak containing strong α phase and weak β phase. Melting endotherms of EPVDF and TPVDF show a strong melting peak at 166.4 ℃ and 165.6 ℃, separately. The crystallinity decreases to 21.6% and 20.1%, respectively. Meanwhile, PVDF showed a new β-phase peak at 181.3°C, which was attributed to ethanol and Tween 80 effect on the melting point, crystallinity and crystallite shapes.

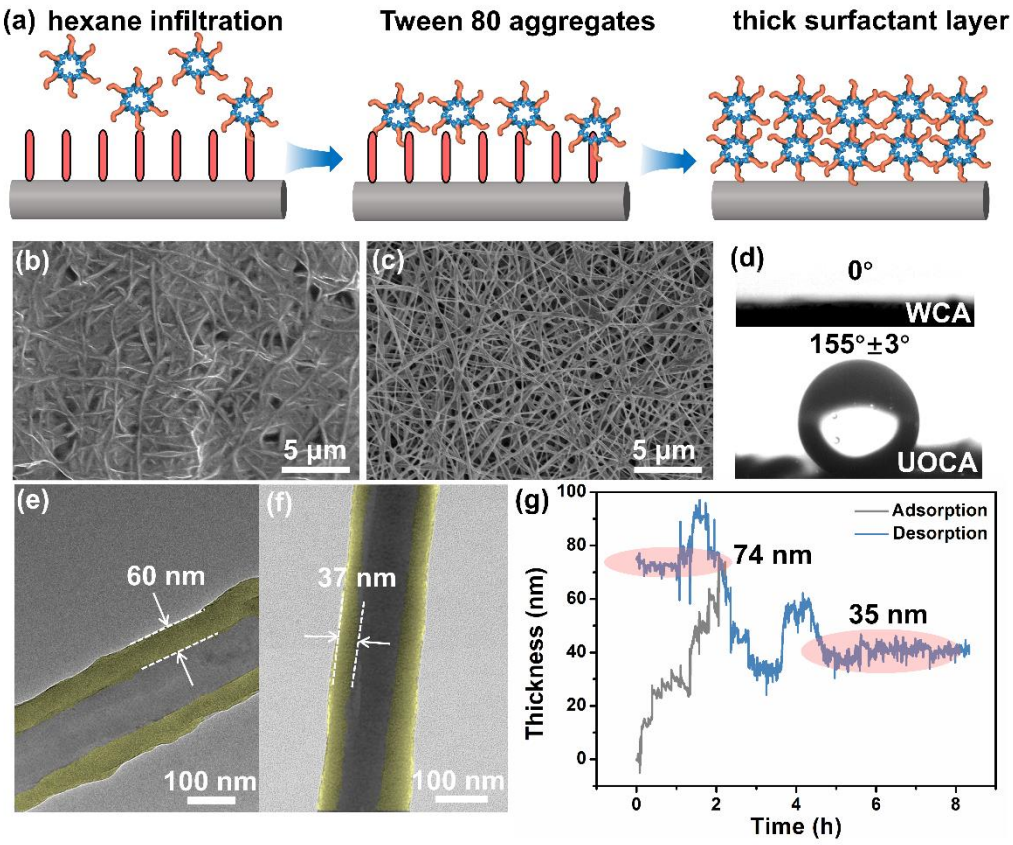

Figure 4. (a) Tween 80 was aggregated on the surface of hydrophobic PVDF nanofiber in hexane solution to form a thick surfactant layer. SEM images of HTPVDF membrane before (b) and after cleaning (c). (d) Air and underwater contact angles of HTPVDF membrane. TEM images of HTPVDF membrane before (e) and after cleaning (f). (g) Adsorption and desorption of Tween 80 onto PVDF nanofibrous membrane in hexane measured by QCM-D. The yellow stained area is the Tween 80 layer.

3.2. Effect of solvent on superhydrophilic and underwater superoleophilic interface construction.

As discussed above, ethanol played an important role in Tween 80 assembly on PVDF nanofiber surface. Solvent that can be used in this process must satisfy two prerequisites: 1) the solvent can wet PVDF nanofibrous membrane and 2) dissolve or disperse Tween 80. PVDF nanofibrous membrane was hydrophobic, therefore, it can

be wetted using either low surface tension polar solvent (e.g., alcohols) or low surface tension non-polar solvent (e.g., hexane, Figure S12a, Supporting Information). However, Tween 80 cannot be dissolved in hexane, which caused Tween 80 aggregates dispersed in hexane (Figure S12b, Supporting Information). Meanwhile, hydrophobic segments were exposed to the hexane solvent and hydrophilic segments trapped in the center of the aggregates (Figure 4a). Thus, a welded nanofiber structure with much crosslinking point between nanofibers was obtained (Figure 4b). By further thorough cleaning with water for 24 h, few weld structure appeared. PVDF nanofibrous membrane is hydrophilic and underwater superoleophobic (Figure 4d, WCA=0^{o}, UOCA=155^{o}±3^{o}) due to the presence of thick Tween 80 layer on PVDF nanofiber (60 nm after filtration and 37 nm after cleaning, Figure 4e and 4f, Figure S13, Supporting Information) on PVDF nanofiber. Equally, after 2 h of adsorption (Tween 80/hexane) and 8 h of desorption (water) using QCM-D, the initial thickness of Tween 80 was 74 nm and the final thickness was 35 nm (Figure 4g), which was basically consistent with the results of TEM results.

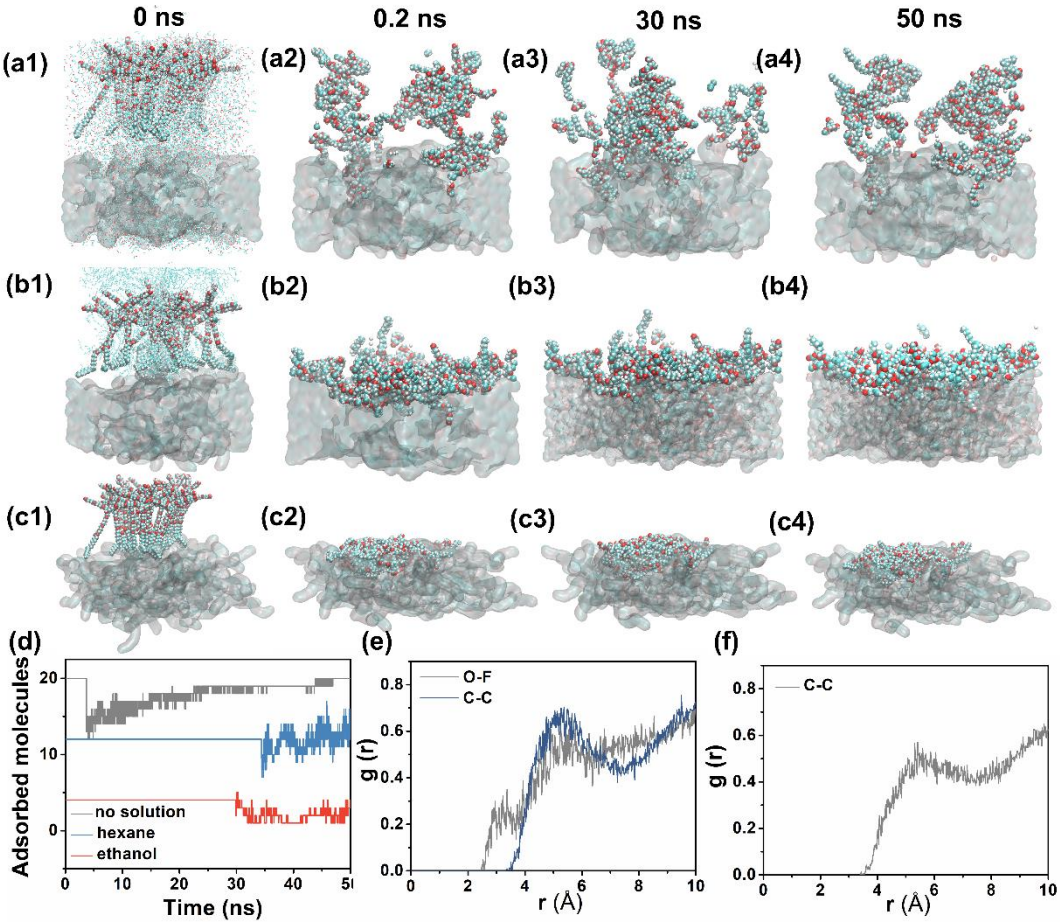

Figure 5. MD models of Tween 80 molecular formation on PVDF polymers at different time for (a1-a4) Tween80/ethanol, (b1-b4) Tween 80/hexane and (c1-c4) Tween 80. White, red, cyan and pink colors represent the H, O, C and F atoms, respectively. (d) Number of adsorbed Tween 80 molecules within 1 nm from the surface of PVDF for Tween80/ethanol, Tween 80/hexane and Tween 80. (e) Radial pair distribute function of O-F and C-C pairs between ethanol and PVDF. (f) Radial pair distribute function of C-C pairs between hexane and PVDF.

To further reveal the underlying effect of solvent on Tween 80 deposition thickness, we performed MD simulations with Tween 80-solvent (ethanol and hexane)-deposited PVDF. Figure 5a1-a4 show the snapshots in the deposition process of Tween 80 in ethanol solution on the PVDF surface. The results indicate that few Tween 80 molecules were deposited/embedded on the PVDF surface and most of them went into ethanol solution, which agrees well with our experimental

observations. However, when ethanol was replaced with hexane or pure Tween 80 was used, almost all Tween 80 molecules are deposited on PVDF surface in Figure 5b, c.

To quantitatively analyze the deposition process of Tween 80 on PVDF, the number of adsorbed Tween 80 molecules (within 1 nm distance from PVDF top surface) during the deposition process was recorded (Figure 5d). It indicated that pure Tween 80 has 20 molecules adsorbed on PVDF in 5 ns (all the added Tween 80 was adsorbed), Tween 80/hexane has 15 Tween 80 molecules adsorbed on PVDF in 34 ns and the Tween 80/ethanol has only 4 Tween 80 molecules adsorbed on PVDF in 30 ns. From the radial distribution function, the CH_3CH_2 group in ethanol has a significant hydrophobic interaction with PVDF, which is in contrast to OH in ethanol (Figure 5e). Therefore, PVDF has a hydrophobic interaction with the CH_3CH_2 group of ethanol with its OH group facing outwards, preventing the hydrophobic group of Tween 80 from interacting with PVDF and resulting in few numbers of Tween 80 being deposited on PVDF. In contrast, the alkane chain of n-hexane promotes the interaction of the hydrophobic segment of Tween 80 with PVDF, increasing the amount of Tween 80 adsorbed (Figure 5f).

To further verify this phenomenon, we conducted polydopamine coating on PVDF nanofibrous membrane due to its well relationship between coating time and coating thickness[67]. Results in Figure S14a, Supporting Information, indicated that PVDF nanofibrous membrane with superhydrophilic and underwater superoleophilic property can be obtained when dopamine coating time was less than 1 min. However, if the coating time was longer than 1 min, superhydrophilic and underwater superoleophobic property was obtained (Figure S14b, Supporting Information, WCA=0°, UOCA=143°±4°). Since the chemical structure of polydopamine layer is unlikely to change in a few s minutes, the main reason might be the difference in thickness (Figure S14c, Supporting Information). As indicated in Figure S14d, Supporting Information, a uniform PDA layer of about 11 nm can be observed, which

is consistent with the previous conclusion. A clear enrichment of O and N element in the outer surface can be observed in Supplementary Figure 14 g, h, while F and C element was mainly distributed on the main nanofiber (Figure S14e, f, Supporting Information).

3.3. Effect of surfactant and substrate on superhydrophilic and underwater superoleophilic interface construction.

Actually, surfactant is a very big family with different hydrophilic and hydrophobic segments. Tween 80 is typical water-soluble surfactant with a HLB value of 15.0. To verify the universality of this strategy to fabricate superhydrophilic and underwater superoleophilic interface, surfactants with different HLB value (1.8-16.7, details can be found in Table S1, Figure S15, 16, Supporting Information) were evaluated. Results showed that superhydrophilic and underwater superoleophilic property can be obtained for surfactants with HLB value higher than 4.3 (e.g., Tween 20: 16.7, Tween 80: 15.0, Tween 85: 11.0 and Span 20: 8.6, Figure S17, Supporting Information). Water contact angle of Span 80 (HLB: 4.3) and Span 85 (HLB: 1.8) treated membrane was 107°±2° and 130°±3° respectively, failing to achieve the above abnormal wetting property.

Moreover, different hydrophobic nanofibrous membranes (PSF, PU, PCL and PS) could be modified by ultrathin hydrophilic layer strategy to achieve superhydrophilic and underwater superoleophilic property (Table S2, Figure S18, 19, Supporting Information), verifying the universality of this strategy.

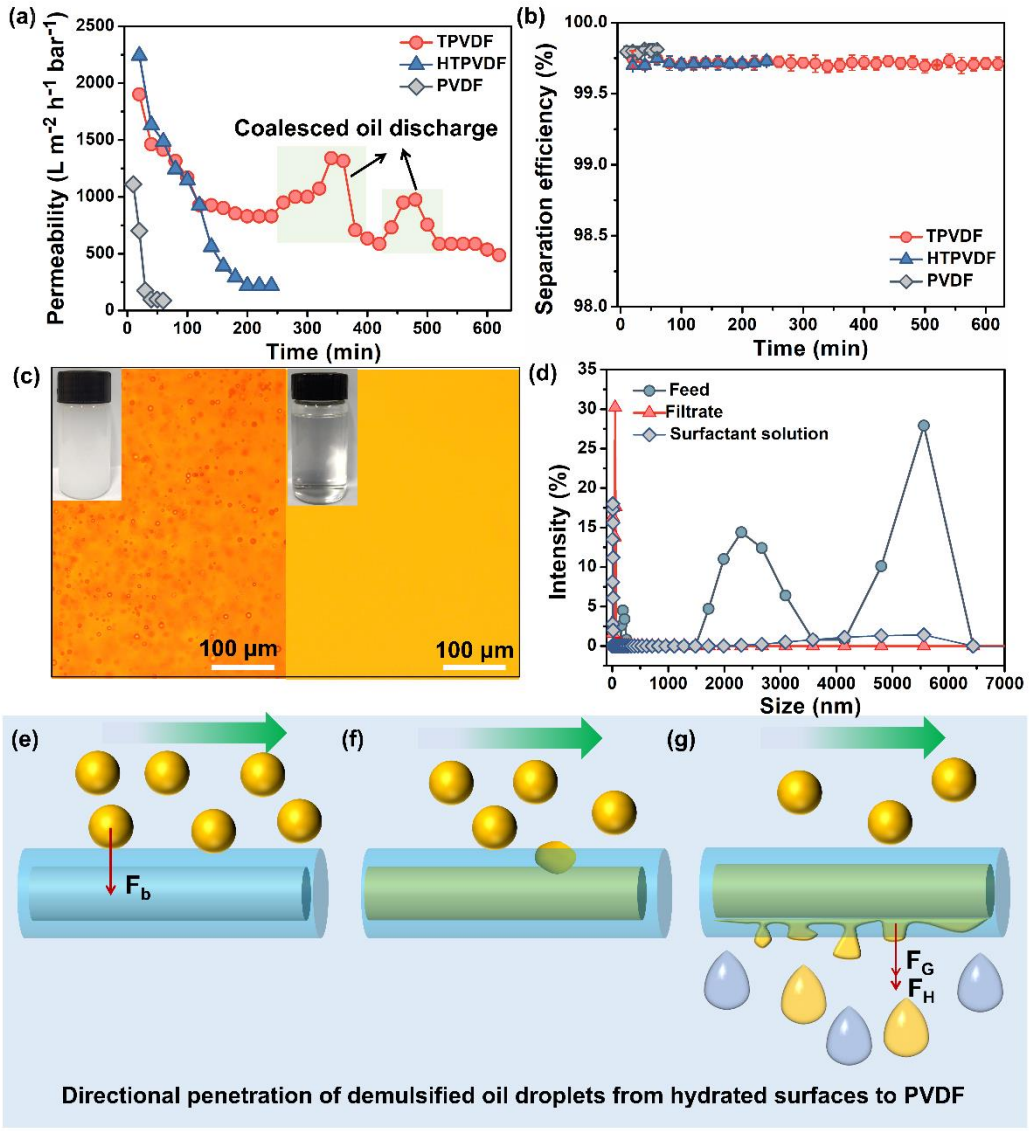

Figure 6. Permselectivity of TPVDF nanofibrous membranes. (a) Permeability and (b) separation efficiency of TPVDF, HTPVDF and PVDF membrane for hexane-in-water emulsion. (c) Optical images of the feed and filtrate solution. (d) Particle size distribution of surfactant, feed liquid and filtrate. (e-g) Schematic illustration of oil-water separation mechanism for TPVDF membrane.

3.4. Separation performance and antifouling mechanism of membrane.

Separation performance of the fabricated membrane for oil-in-water emulsion was evaluated (Figure S20, Supporting Information). After separation, milky emulsion was separated into incompatible aqueous phase and oil phase. Figure 6a showed that initial

water permeability of TPVDF (around 1901 L m^{-2} h^{-1} bar^{-1}) and HTPVDF (around 2242 L m^{-2} h^{-1} bar^{-1}) membrane was much higher than PVDF (around 1111.4 L m^{-2} h^{-1} bar^{-1}) membrane. Hydrophobic PVDF nanofibrous membrane was transformed into superhydrophilic membrane due to the self-assembly of Tween 80, where hydrophilic fragments are exposed to the external environment at the interface of PVDF nanofibers. These hydrophilic groups make the membrane hydrophilic, which is beneficial for promoting the rapid water flow. TPVDF and HTPVDF exhibit superhydrophilicity in air, which is conducive to continuous water phase entering the membrane and improving water permeability during the separation of oil in water emulsion (as shown in Figure 1 and 4). Moreover, permeability of PVDF membrane was rapidly decreased within 10 min due to the strong affinity between PVDF and oils and therefore membrane pores were blocked. Benefiting from the unique "oil-water-receiving" properties, the permeability of the TPVDF membrane remained as high as 500 L m^{-2} h^{-1} bar^{-1} even after 10 h of continuous separation, although permeability of TPVDF membrane was also declined. Oil passes through the membrane and floats on the aqueous phase of the filtrate, making the layered oil-water mixture easy to separate (Figure S21, Supporting Information). The rise in permeation flux was due to the outflow of accumulated oil droplets away from the membrane. Besides, the TPVDF membrane also showed favorable separation performances for hexadecane-in-water emulsion, D5-in-water emulsion and dodecane-in-water emulsion (Figure S22, Supporting Information). The TPVDF membrane showed highly separation efficiency for various emulsions (> 99.2%). And the permeability of the membrane slightly decreases due to the increase in oil viscosity. Compared with HTPVDF and other membranes, few membranes could operate continuously for 10 h (Table S3). Permeability of HTPVDF membrane decreased to near zero in about 200 min due to membrane pore was blocked by oil droplets. Separation efficiency of all membranes was greater than 99.5% (Figure 6b). The milky feed emulsion solution with numerous oil droplets turns into transparent filtrate solution in water phase (Figure 6c). Particle size distribution in the filtrate is consistent with that of surfactant solution, indicating

that the surfactant in emulsion enters the filtrate solution (Figure 6d). PVDF membranes modified by surfactants with different HLB values also showed excellent separation performance (Figure S23, Supporting Information). Such an excellent antifouling performance was mainly attributed to the superhydrophilic and underwater superoleophilic property of TPVDF membrane. Firstly, the membrane was prewetted by water to form a hydrated layer on membrane surface due to its superhydrophilic property, which could allow the water phase to permeate through freely. Secondly, the underwater superoleophilic property benefited the oil capture (demulsification) from oil-in water emulsion solution. Once the emulsified oils got into the membrane, they can easily pass through the hydrated layer due to the Laplace force (directional penetration) and coalesced on the hydrophobic PVDF nanofiber (Figure 6e). Finally, the coalesced oil droplets leaved the PVDF nanofiber by the applied hydration pressure. Dispersed oil droplets were diverted beneath the ultra-thin hydrophilic layer and captured by PVDF bulk to form coalesced oil phase and discharged out of the nanofibrous membrane as continuous macroscopic oil phase. Therefore, water and emulsified oil transport across the membrane without mutual interference. However, the oil phase cannot be completely transferred from PVDF nanofibers due to the high affinity of PVDF nanofibers for the oil phase. Therefore, the flux recovery is low after oil removal (Figure S24, Supporting Information). The independent transport pathway sorted out the common membrane fouling issue for oil/water separation, which is a totally different oil/water separation mechanism form previously reported superwetting membranes.

4. Conclusion

Poly (vinylidene fluoride) nanofibrous membrane with superhydrophilic and underwater superoleophilic property for enhanced membrane antifouling was fabricated. The obtained membrane exhibited high permeability and emulsion treatment capacity for surfactant-stabilized oil-in-water emulsions based on a coalescence demulsification mechanism. High emulsion treatment capacity was

realized by preventing hydration layer contamination on membrane surface and in membrane pores. Water and emulsified oils can penetrate in membrane much easier ("oil-water-receiving" membrane). Meanwhile, emulsified oils were collected and transported beneath the ultra-thin hydrophilic layer and captured by hydrophobic PVDF bulk to form coalesced oil phase and discharged out of the nanofibrous membrane as continuous macroscopic oil phase. The optimized TPVDF nanofibrous membrane showed long-lasting permeability (10 h) for emulsions. The ultrathin hydrophilic layer strategy offered new understanding for coalescence demulsification and might advance its practical applications.

Acknowledgements

This work is financially supported by National Natural Science Foundation of China (Grant No. 22205248), China Postdoctoral Science Foundation (2022M713240), Natural Science Foundation of Ningbo (2022J303), "Science and Technology Innovation 2025" Major Project of Ningbo (2020Z105), Nature Science Foundation of Ningbo-Key Project (202003N4031), Zhejiang Provincial Natural Science Foundation of China for Distinguished Young Scholars (LR20E030002), Ten thousand plan-high level talents special support plan of Zhejiang province, China (ZJWR0108020). Thanks to Dr. Zhe Yang of the University of Hong Kong for providing the QCM-D test and Dr. Nianxiang Qiu for providing simulation data.

Conflict of Interest

The authors declare no conflict of interest.

References

[1] X. Wang, J. Yu, G. Sun, B. Ding, Electrospun Nanofibrous Materials: A Versatile Medium for Effective Oil/Water Separation, Mater. Today, 19 (2016) 403-414.

[2] S. Zarghami, T. Mohammadi, M. Sadrzadeh, B. Van der Bruggen, Superhydrophilic and Underwater Superoleophobic Membranes - a Review of Synthesis Methods, Prog. Polym. Sci., 98 (2019) 101166.

[3] E. Tummons, Q. Han, H. Tanudjaja, C. Hejase, J. Chew, V. Tarabara, Membrane Fouling by

578 Emulsified Oil: A Review, Sep. Purif. Technol., 248 (2020) 116919.
579 [4] H.J. Tanudjaja, C.A. Hejase, V.V. Tarabara, A.G. Fane, J.W. Chew, Membrane-Based Separation for
580 Oily Wastewater: A Practical Perspective, Water Res., 156 (2019) 347-365.
581 [5] D. Dong, Y. Zhu, W. Fang, M. Ji, A. Wang, S. Gao, H. Lin, R. Huang, J. Jin, Double- Defense
582 Design of Super- Anti- Fouling Membranes for Oil/Water Emulsion Separation, Adv. Funct. Mater.,
583 (2022) 2113247.
584 [6] B. Wang, X. Luo, Y. Feng, L. Yang, C. Zhang, Z. Dong, L. Jiang, H. Dai, Turbo-Synergistic Oily
585 Wastewater Remediation in Bio-Inspired Cone Array Barrel, Adv. Sci., 9 (2022) 2204244.
586 [7] Y. Zhao, Y. Gu, G. Gao, Piezoelectricity Induced by Pulsed Hydraulic Pressure Enables in Situ
587 Membrane Demulsification and Oil/Water Separation, Water Res., 215 (2022) 118245.
588 [8] Q. Lin, G. Zeng, G. Yan, J. Luo, X. Cheng, Z. Zhao, H. Li, Self-Cleaning Photocatalytic Mxene
589 Composite Membrane for Synergistically Enhanced Water Treatment: Oil/Water Separation and Dyes
590 Removal, Chem. Eng. J., 427 (2022) 131668.
591 [9] T. Zsirai, P. Buzatu, P. Aerts, S. Judd, Efficacy of Relaxation, Backflushing, Chemical Cleaning and
592 Clogging Removal for an Immersed Hollow Fibre Membrane Bioreactor, Water Res., 46 (2012) 4499-
593 4507.
594 [10] E. Mavredaki, A. Stathoulopoulou, E. Neofotistou, K.D. Demadis, Environmentally Benign
595 Chemical Additives in the Treatment and Chemical Cleaning of Process Water Systems: Implications
596 for Green Chemical Technology, Desalination, 210 (2007) 257-265.
597 [11] Y. Liu, Y. Su, J. Guan, J. Cao, R. Zhang, M. He, K. Gao, L. Zhou, Z. Jiang, 2d Heterostructure
598 Membranes with Sunlight-Driven Self Cleaning Ability for Highly Efficient Oil–Water Separation, Adv.
599 Funct. Mater., 28 (2018) 1706545.
600 [12] A. Xie, J. Cui, J. Yang, Y. Chen, J. Dai, J. Lang, C. Li, Y. Yan, Photo-Fenton Self-Cleaning
601 Membranes with Robust Flux Recovery for an Efficient Oil/Water Emulsion Separation, J. Mater.
602 Chem. A, 7 (2019) 8491-8502.
603 [13] Y.H. Cai, D.Y. Chen, N.J. Li, Q.F. Xu, H. Li, J.H. He, J.M. Lu, A Self-Cleaning Heterostructured
604 Membrane for Efficient Oil-in-Water Emulsion Separation with Stable Flux, Adv. Mater., 32 (2020)
605 2001265.
606 [14] H.R. Zhang, A.U. Mane, X.B. Yang, Z.J. Xia, E.F. Barry, J.Q. Luo, Y.H. Wan, J.W. Elam, S.B.
607 Darling, Visible-Light-Activated Photocatalytic Films toward Self-Cleaning Membranes, Adv. Funct.
608 Mater., 30 (2020) 2002847.
609 [15] Y. Yang, S. Qiao, J.T. Zhou, X. Quan, Mitigating Membrane Fouling Based on in Situ Center Dot
610 Oh Generation in a Novel Electro-Fenton Membrane Bioreactor, Environ. Sci. Technol., 54 (2020)
611 7669-7676.
612 [16] J.Q. Sun, C.Z. Hu, B.C. Wu, J.H. Qu, Fouling Mitigation of a Graphene Hydrogel Membrane
613 Electrode by Electrical Repulsion and in Situ Self-Cleaning in an Electro-Membrane Reactor, Chem.
614 Eng. J., 393 (2020) 124817.
615 [17] D.N. Pei, C. Liu, A.Y. Zhang, X.Q. Pan, H.Q. Yu, In Situ Organic Fenton-Like Catalysis Triggered
616 by Anodic Polymeric Intermediates for Electrochemical Water Purification, Proc. Natl. Acad. Sci. U. S.
617 A., 117 (2020) 30966-30972.
618 [18] Y. Wang, J. Wang, Y. Ding, S. Zhou, F. Liu, In Situ Generated Micro-Bubbles Enhanced
619 Membrane Antifouling for Separation of Oil-in-Water Emulsion, J. Membr. Sci., 621 (2021) 119005.
620 [19] E. Lee, Y. Kim, M. Jeon, H. Kim, The Effect of Aeration Types on Foulant Removal in Ex-Situ
621 Chemical Cleaning in Place (Cip) with Membranes Fouled by Secondary Effluents, Chem. Eng. J., 333

(2018) 730-738.
[20] R. Li, L. Rao, J. Zhang, L. Shen, Y. Xu, X. You, B.-Q. Liao, H. Lin, Novel in-Situ Electroflotation Driven by Hydrogen Evolution Reaction (Her) with Polypyrrole (Ppy)-Ni-Modified Fabric Membrane for Efficient Oil/Water Separation, J. Membr. Sci., 635 (2021) 119502.
[21] Z. Zhu, W. Wang, D. Qi, Y. Luo, Y. Liu, Y. Xu, F. Cui, C. Wang, X. Chen, Calcinable Polymer Membrane with Revivability for Efficient Oily-Water Remediation, Adv. Mater., 30 (2018) 1801870.
[22] D. Li, W. Xu, Y. Mu, H. Yu, H. Jiang, J. Crittenden, Remediation of Petroleum-Contaminated Soil and Simultaneous Recovery of Oil by Fast Pyrolysis, Environ. Sci. Technol., 52 (2018) 5330-5338.
[23] N.M. Kocherginsky, C.L. Tan, W.F. Lu, Demulsification of Water-in-Oil Emulsions Via Filtration through a Hydrophilic Polymer Membrane, J. Membr. Sci., 220 (2003) 117-128.
[24] M. Kukizaki, M. Goto, Demulsification of Water-in-Oil Emulsions by Permeation through Shirasu-Porous-Glass (Spg) Membranes, J. Membr. Sci., 322 (2008) 196-203.
[25] X.F. You, Y. Liao, M. Tian, J.W. Chew, R. Wang, Engineering Highly Effective Nanofibrous Membranes to Demulsify Surfactant-Stabilized Oil-in-Water Emulsions, J. Membr. Sci., 611 (2020) 118398.
[26] X. Zhu, L. Zhu, H. Li, C.Y. Zhang, J.W. Xue, R. Wang, X.R. Qiao, Q.Z. Xue, Enhancing Oil-in-Water Emulsion Separation Performance of Polyvinyl Alcohol Hydrogel Nanofibrous Membrane by Squeezing Coalescence Demulsification, J. Membr. Sci., 630 (2021) 119324.
[27] J. Wang, B. He, Y. Ding, T. Li, W. Zhang, Y. Zhang, F. Liu, C. Tang, Beyond Superwetting Surfaces: Dual-Scale Hyperporous Membrane with Rational Wettability for "Nonfouling" Emulsion Separation Via Coalescence Demulsification, ACS Appl. Mater. Interfaces, 13 (2021) 4731-4739.
[28] Y. Ding, B. Hu, L. Zhuang, J. Wang, J. Wu, F. Liu, J. Wang, Confined Channels Induced Coalescence Demulsification and Slippery Interfaces Constructed Fouling Resist-Release for Long-Lasting Oil/Water Separation, ACS Appl. Mater. Interfaces, 13 (2021) 30224-30234.
[29] Y. Zhu, J. Wang, F. Zhang, S. Gao, A. Wang, W. Fang, J. Jin, Zwitterionic Nanohydrogel Grafted Pvdf Membranes with Comprehensive Antifouling Property and Superior Cycle Stability for Oil-in-Water Emulsion Separation, Adv. Funct. Mater., 28 (2018) 1804121.
[30] X. Zhao, Y. Su, J. Cao, Y. Li, R. Zhang, Y. Liu, Z. Jiang, Fabrication of Antifouling Polymer–Inorganic Hybrid Membranes through the Synergy of Biomimetic Mineralization and Nonsolvent Induced Phase Separation, J. Mater. Chem. A, 3 (2015) 7287-7295.
[31] S.X. Zhang, G.S. Jiang, S.J. Gao, H.L. Jin, Y.Z. Zhu, F. Zhang, J. Jin, Cupric Phosphate Nanosheets-Wrapped Inorganic Membranes with Superhydrophilic and Outstanding Anticrude Oil-Fouling Property for Oil/Water Separation, ACS Nano, 12 (2018) 795-803.
[32] L. Hou, N. Wang, J. Wu, Z. Cui, L. Jiang, Y. Zhao, Bioinspired Superwettability Electrospun Micro/Nanofibers and Their Applications, Adv. Funct. Mater., 28 (2018) No.1801114.
[33] Y. Lu, Y. Zhu, F. Yang, Z. Xu, Q. Liu, Advanced Switchable Molecules and Materials for Oil Recovery and Oily Waste Cleanup, Adv. Sci., 8 (2021) 2004082.
[34] J. Wu, Y. Ding, J. Wang, T. Li, H. Lin, J. Wang, F. Liu, Facile Fabrication of Nanofiber- and Micro/Nanosphere-Coordinated Pvdf Membrane with Ultrahigh Permeability of Viscous Water-in-Oil Emulsions, J. Mater. Chem. A, 6 (2018) 7014-7020.
[35] S. Plimpton, Fast Parallel Algorithms for Short-Range Molecular Dynamics, J. Comput. Phys., 117 (1995) 1-19.
[36] A.D. William Humphrey, Klaus Schulten, Vmd: Visual Molecular Dynamics, J. Mol. Graphics, 14 (1996) 33-38.

[37] L. Martinez, R. Andrade, E.G. Birgin, J.M. Martinez, Packmol: A Package for Building Initial Configurations for Molecular Dynamics Simulations, J. Comput. Chem., 30 (2009) 2157-2164.
[38] R.W. Hockney, Eastwood, J.W, Computer Simulation Using Particles, CRC Press, 87 (1988) 28779.
[39] B. Leimkuhler, E. Noorizadeh, O. Penrose, Comparing the Efficiencies of Stochastic Isothermal Molecular Dynamics Methods, J. Stat. Phys., 143 (2011) 921-942.
[40] H.J.C. Berendsen, J.P.M. Postma, W.F. van Gunsteren, A. DiNola, J.R. Haak, Molecular Dynamics with Coupling to an External Bath, J. Chem. Phys., 81 (1984) 3684-3690.
[41] J.T.-R. William L. Jorgensen, Potential Energy Functions for Atomic-Level Simulations Ofwater and Organic and Biomolecular Systems, PNAS, 102 (2005) 6665–6670.
[42] L.S. Dodda, J.Z. Vilseck, J. Tirado-Rives, W.L. Jorgensen, 1.14*Cm1a-Lbcc: Localized Bond-Charge Corrected Cm1a Charges for Condensed-Phase Simulations, J. Phys. Chem. B, 121 (2017) 3864-3870.
[43] A.K. Malde, L. Zuo, M. Breeze, M. Stroet, D. Poger, P.C. Nair, C. Oostenbrink, A.E. Mark, An Automated Force Field Topology Builder (Atb) and Repository: Version 1.0, J. Chem. Theory Comput., 7 (2011) 4026-4037.
[44] M. Tao, L. Xue, F. Liu, L. Jiang, An Intelligent Superwetting Pvdf Membrane Showing Switchable Transport Performance for Oil/Water Separation, Adv. Mater., 26 (2014) 2943-2948.
[45] S. Gao, J. Sun, P. Liu, F. Zhang, W. Zhang, S. Yuan, J. Li, J. Jin, A Robust Polyionized Hydrogel with an Unprecedented Underwater Anti-Crude-Oil-Adhesion Property, Adv. Mater., 28 (2016) 5307-5314.
[46] W. Lv, Q. Mei, J. Xiao, M. Du, Q. Zheng, 3d Multiscale Superhydrophilic Sponges with Delicately Designed Pore Size for Ultrafast Oil/Water Separation, Adv. Funct. Mater., 27 (2017) 1704293.
[47] J.C. Zhang, L.F. Liu, Y. Si, J.Y. Yu, B. Ding, Electrospun Nanofibrous Membranes: An Effective Arsenal for the Purification of Emulsified Oily Wastewater, Adv. Funct. Mater., 30 (2020) 2002192.
[48] Z.X. Bai, K. Jia, C.C. Liu, L.L. Wang, G. Lin, Y.M. Huang, S.N. Liu, X.B. Liu, A Solvent Regulated Hydrogen Bond Crosslinking Strategy to Prepare Robust Hydrogel Paint for Oil/Water Separation, Adv. Funct. Mater., 31 (2021) 2104701.
[49] G.M. Meconi, N. Ballard, J.M. Asua, R. Zangi, Adsorption and Desorption Behavior of Ionic and Nonionic Surfactants on Polymer Surfaces, Soft Matter, 12 (2016) 9692-9704.
[50] A. Zdziennicka, B. Janczuk, Modification of Adsorption, Aggregation and Wetting Properties of Surfactants by Short Chain Alcohols, Adv. Colloid Interface Sci., 284 (2020) 102249.
[51] N. Chithralekha, A. Panneerselvam, Surfactant - Alcohol Interactions: An Ultrasonic, Uv and Ftir Analysis, Vacuum, 168 (2019) 108835.
[52] S. Gao, Y. Zhu, J. Wang, F. Zhang, J. Li, J. Jin, Layer-by-Layer Construction of Cu2+/Alginate Multilayer Modified Ultrafiltration Membrane with Bioinspired Superwetting Property for High-Efficient Crude-Oil-in-Water Emulsion Separation, Adv. Funct. Mater., 28 (2018) 1801944.
[53] H.C. Yang, Y.S. Xie, H. Chan, B. Narayanan, L. Chen, R.Z. Waldman, S.K.R.S. Sankaranarayanan, J.W. Elam, S.B. Darling, Crude-Oil-Repellent Membranes by Atomic Layer Deposition: Oxide Interface Engineering, ACS Nano, 12 (2018) 8678-8685.
[54] X.B. Yang, P. Sun, H.R. Zhang, Z.J. Xia, R.Z. Waldman, A.U. Mane, J.W. Elam, L. Shao, S.B. Darling, Polyphenol-Sensitized Atomic Layer Deposition for Membrane Interface Hydrophilization, Adv. Funct. Mater., 30 (2020) 1910062.
[55] X.Q. Cheng, Y. Jiao, Z.K. Sun, X.B. Yang, Z.J. Cheng, Q. Bai, Y.J. Zhang, K. Wang, L. Shao,

Constructing Scalable Superhydrophobic Membranes for Ultrafast Water-Oil Separation, ACS Nano, 15 (2021) 3500-3508.
[56] X.S. Xie, Z.Z. Zheng, X.Q. Wang, D.L. Kaplan, Low-Density Silk Nanofibrous Aerogels: Fabrication and Applications in Air Filtration and Oil/Water Purification, ACS Nano, 15 (2021) 1048-1058.
[57] J. Jin, H. Wang, Y. Jing, M. Liu, D. Wang, Y. Li, M. Bao, An Efficient and Environmental-Friendly Dispersant Based on the Synergy of Amphiphilic Surfactants for Oil Spill Remediation, Chemosphere, 215 (2019) 241-247.
[58] V. Krstonošić, M. Milanović, L. Dokić, Application of Different Techniques in the Determination of Xanthan Gum-Sds and Xanthan Gum-Tween 80 Interaction, Food Hydrocolloids, 87 (2019) 108-118.
[59] C.V.H. Chen, Y. Liu, H.A. Stone, R.K. Prud'homme, Visualization of Surfactant Dynamics to and Along Oil-Water Interfaces Using Solvatochromic Fluorescent Surfactants, Langmuir, 34 (2018) 10512-10522.
[60] F. Orudzhev, S. Ramazanov, D. Sobola, P. Kaspar, T. Trcka, K. Castkova, J. Kastyl, I. Zvereva, C.Y. Wang, D. Selimov, R. Gulakhmedov, M. Abdurakhmanov, A. Shuaibov, M. Kadiev, Ultrasound and Water Flow Driven Piezophototronic Effect in Self-Polarized Flexible Alpha-Fe2o3 Containing Pvdf Nanofibers Film for Enhanced Catalytic Oxidation, Nano Energy, 90 (2021) 106586.
[61] S. Cheon, H. Kang, H. Kim, Y. Son, J.Y. Lee, H.J. Shin, S.W. Kim, J.H. Cho, High-Performance Triboelectric Nanogenerators Based on Electrospun Polyvinylidene Fluoride-Silver Nanowire Composite Nanofibers, Adv. Funct. Mater., 28 (2018) 1703778.
[62] G. Mago, D.M. Kalyon, F.T. Fisher, Membranes of Polyvinylidene Fluoride and Pvdf Nanocomposites with Carbon Nanotubes Via Immersion Precipitation, J. Nanomater., 2008 (2008) 759825.
[63] P. Sukitpaneenit, T.-S. Chung, Molecular Elucidation of Morphology and Mechanical Properties of Pvdf Hollow Fiber Membranes from Aspects of Phase Inversion, Crystallization, and Rheology, in: Hollow Fiber Membr., 2021, pp. 333-360.
[64] M. Ishiguro, L.K. Koopal, Surfactant Adsorption to Soil Components and Soils, Adv. Colloid Interface Sci., 231 (2016) 59-102.
[65] W. Zhu, F.S. Romanski, X. Meng, S. Mitra, M.S. Tomassone, Atomistic Simulation Study of Surfactant and Polymer Interactions on the Surface of a Fenofibrate Crystal, Eur. J. Pharm. Sci., 42 (2011) 452-461.
[66] A. Barati-Harooni, A. Najafi-Marghmaleki, A. Tatar, A.H. Mohammadi, Experimental and Modeling Studies on Adsorption of a Nonionic Surfactant on Sandstone Minerals in Enhanced Oil Recovery Process with Surfactant Flooding, J. Mol. Liq., 220 (2016) 1022-1032.
[67] H. Lee, S.M. Dellatore, W.M. Miller, P.B. Messersmith, Mussel-Inspired Surface Chemistry for Multifunctional Coatings, Science, 318 (2007) 426.